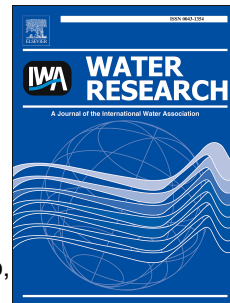


Accepted Manuscript



Activation of persulfates by natural magnetic pyrrhotite for water disinfection:
Efficiency, mechanisms, and stability

Dehua Xia, Yan Li, Guocheng Huang, Ran Yin, Taicheng An, Guiying Li, Huijun Zhao,
Anhuai Lu, Po Keung Wong

PII: S0043-1354(17)30059-3

DOI: [10.1016/j.watres.2017.01.052](https://doi.org/10.1016/j.watres.2017.01.052)

Reference: WR 12653

To appear in: *Water Research*

Received Date: 25 November 2016

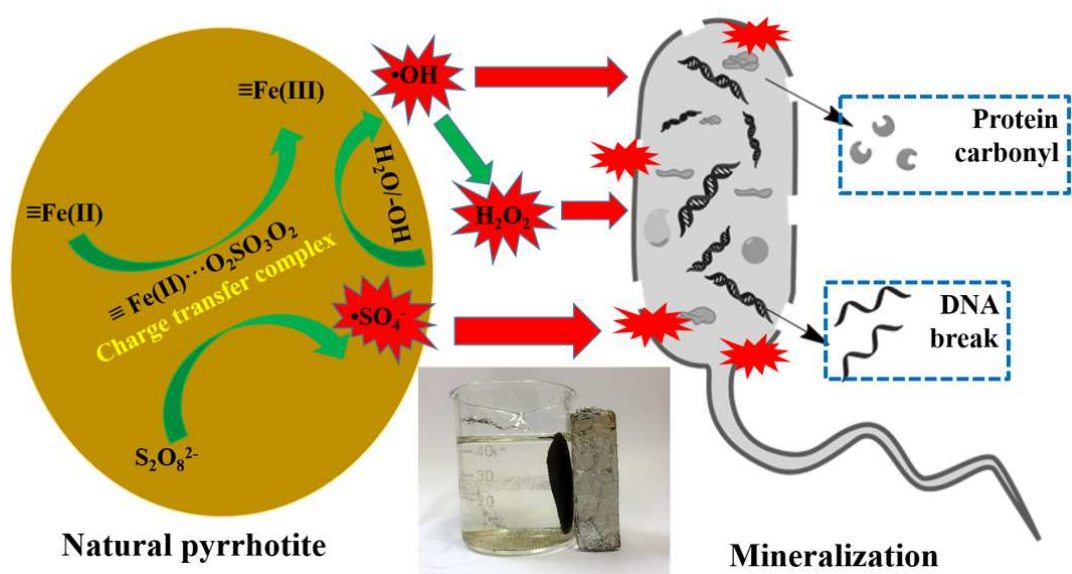
Revised Date: 21 January 2017

Accepted Date: 25 January 2017

Please cite this article as: Xia, D., Li, Y., Huang, G., Yin, R., An, T., Li, G., Zhao, H., Lu, A., Wong, P.K.,
Activation of persulfates by natural magnetic pyrrhotite for water disinfection: Efficiency, mechanisms,
and stability, *Water Research* (2017), doi: 10.1016/j.watres.2017.01.052.

This is a PDF file of an unedited manuscript that has been accepted for publication. As a service to
our customers we are providing this early version of the manuscript. The manuscript will undergo
copyediting, typesetting, and review of the resulting proof before it is published in its final form. Please
note that during the production process errors may be discovered which could affect the content, and all
legal disclaimers that apply to the journal pertain.

Graphical Abstract



1 **Activation of Persulfates by Natural Magnetic Pyrrhotite for Water Disinfection:**
2 **Efficiency, Mechanisms, and Stability**

3

4 Dehua Xia ^a, Yan Li ^b, Guocheng Huang ^a, Ran Yin ^c, Taicheng An ^{d,**}, Guiying Li ^d,
5 Huijun Zhao ^{e, f}, Anhuai Lu ^g, Po Keung Wong ^{a,*}

6

7 ^a School of Life Sciences, The Chinese University of Hong Kong, Shatin, NT, Hong
8 Kong SAR, China

9 ^b The Key Laboratory of Orogenic Belts and Crustal Evolution, School of Earth and
10 Space Sciences, Peking University, Beijing 100871, China

11 ^c Department of Civil and Environmental Engineering, The Hong Kong University of
12 Science and Technology, Clear Water Bay, Kowloon, Hong Kong SAR, China

13 ^d Institute of Environmental Health and Pollution Control, School of Environmental
14 Science and Engineering, Guangdong University of Technology, Guangzhou
15 510006, Guangdong, China

16 ^e Centre for Clean Environment and Energy, Griffith Scholl of Environment, Griffith
17 University, Queensland 4222, Australia

18 ^f Laboratory of Nanomaterials and Nanostructures, Institute of Solid State Physics,
19 Chinese Academy of Sciences, Hefei 230031, Anhui, China

20 ^g School of Geoscience and Info-Physics, Central South University, Changsha 410083,
21 China

22 Corresponding authors

23

Tel: +86 20 2388 3536, Fax: +86 20 8529 1501, E-mail: antc99@gdut.edu.cn (T.C. An); Tel: +852 3943 6383, Fax: +852 2603 5767, E-mail: pkwong@cuhk.edu.hk (P.K. Wong).

24

25

ACCEPTED MANUSCRIPT

26 **Abstract**

27 This study introduces natural occurring magnetic pyrrhotite (NP) as an
28 environmentally friendly, easy available, and cost-effective alternative catalyst to
29 activate persulfate (PS) of controlling microbial water contaminants. The *E. coli* K-12
30 inactivation kinetics observed in batch experiments was well described with
31 first-order reaction. The optimum inactivation rate ($k = 0.47 \text{ log/min}$) attained at a NP
32 dose of 1 g/L and a PS dose of 1 mM, corresponding to total inactivation of 7 log_{10}
33 cfu/mL cells within 15 min. Measured k increased > 2 -fold when temperature
34 increased from 20 to 50 °C; and > 4 -fold when pH decreased from 9 to 3. Aerobic
35 conditions were more beneficial to cell inactivation than anaerobic conditions due to
36 more reactive oxygen species (ROS) generated. ROS responsible for the inactivation
37 were identified to be $\bullet\text{SO}_4^- > \bullet\text{OH} > \text{H}_2\text{O}_2$ based on a positive scavenging test and *in*
38 *situ* ROS determination. *In situ* characterization suggested that PS effectively bind to
39 NP surface was likely to form charge transfer complex ($\equiv\text{Fe(II)}\cdots\text{O}_3\text{SO-OSO}_3^-$),
40 which mediated ROS generation and *E. coli* K-12 oxidation. The increased
41 cell-envelope lesions consequently aggravated intracellular protein depletion and
42 genome damage to cause definite bacterial death. The NP still maintained good
43 physiochemical structure and stable activity even after 4 cycle. Moreover, NP/PS
44 system also exhibited good *E. coli* K-12 inactivation efficiency in authentic water
45 matrices like surface water and effluents of secondary wastewater.

46

47

48 Key words: Natural pyrrhotite, Persulfate, Sulfate radical, Water disinfection,

49 Heterogeneous catalysis

50

51

52

53

54

55

56

57

58

59 **1. Introduction**

60 With increasing populations and uncertain global climate changes, the shortages
61 of fresh and sanitary water require increased water recycle and reuse (Rietveld et al.,
62 2011; Haaken et al., 2014). Biohazards such as bacteria, viruses, and fungi are widely
63 presented in wastewater, which can cause a variety of water-borne diseases to humans
64 and animals (Dobrowsky et al., 2014; Soller et al., 2014). Unfortunately, conventional
65 water disinfection technologies, including chlorination, ozone, and ultraviolet (UV),
66 have some disadvantages during application. For instance, a number of biohazards are
67 naturally resistant to UV and chlorination (Eischeid et al., 2011; Rizzo et al., 2013a,
68 b); the toxic and corrosive characteristics of ozone limit its practical application
69 (Anastasi et al., 2013); the formation of disinfection byproducts (DBPs) by
70 chlorination and ozonation are with potential carcinogenicity or toxicity (Parker et al.,
71 2014; Sharma et al., 2014). Therefore, effectively removing biohazards from water is
72 a challenge that has received great attention (Sun et al., 2014; Huang et al., 2017), and
73 versatile new technologies are highly needed to simultaneously inactivate biohazards
74 and eliminate disinfection debris.

75 In recent decades, sulfate radicals ($\bullet\text{SO}_4^-$) based advanced oxidation process

76 (AOP) has attracted increasing interests in water treatment, due to their high
77 efficiency in degrading a wide range of recalcitrant micro-contaminants (Drzewicz et
78 al., 2012; Yuan et al., 2014) and even inactivating biohazards (Anipsitakis et al., 2008;
79 Tsitonaki et al., 2008; Chesney et al., 2016). For instance, Michael-Kordatou et al.
80 (2015a) evidence that the UVC/PS process can result in rapid and complete
81 erythromycin (ERY) degradation and ERY-resistant *Escherichia coli* inactivation in
82 secondary treated wastewater, thus to produce a final treated effluent with lower
83 phytotoxicity (<10%) compared to the untreated wastewater. The good performance
84 of $\bullet\text{SO}_4^-$ based AOP in wastewater is mainly attributed to the large formation of
85 highly reactive species, such as $\bullet\text{SO}_4^-$ (2.5-3.1 eV) and its derived $\bullet\text{OH}$ (2.7 eV)
86 occurring in natural conditions (Michael-Kordatou et al. 2015a). Moreover, Ahn et al.
87 (2013) use zero valent iron (ZVI) to activate persulfate (PS, $\text{S}_2\text{O}_8^{2-}$) for disinfecting
88 ballast water and achieve a result that the marine phytoplankton could be totally
89 inactivated and mineralized without formation of harmful byproducts. In analogy,
90 $\bullet\text{SO}_4^-$ based AOP may hold promise to be more effective than conventional water
91 disinfection processes in inactivating biohazards due to their more powerful oxidation
92 capabilities and lower tendency to form DBPs.

93 Generally, $\bullet\text{SO}_4^-$ can be produced by the activation of PS and PMS (Wang et al.,
94 2015; Zhong et al., 2015; Feng et al., 2016). Approaches of PS/PMS activation mainly
95 include heat, microwave, UV, and addition of transition metals or carbon materials
96 (Waldemer et al., 2007; Johnson et al., 2008; Guan et al., 2011; Matzek and Carter,
97 2016). Especially, the utilization of transition metal (zero valent iron, Co_3O_4 ,
98 $\text{CuO}/\text{Fe}_3\text{O}_4$, etc.) has received particular attention to heterogeneously activate
99 PS/PMS, because they are not consumed during the activation and no additional
100 energy is required (Guan et al., 2013; Zhang et al., 2013; Zeng et al., 2015; Oh et al.,

101 2016). However, many limitations for the wide-span application of these synthetic
102 catalysts still exist: (1) the complex fabrication procedure and expensive massive
103 production of these catalysts (Wang et al., 2014); (2) the potential leaching of heavy
104 metals in the synthetic catalysts like Co^{2+} or Cu^{2+} are hazardous to environment (Hu
105 et al., 2016; Ren et al., 2015); (3) the recycle and reuse of these nano-size catalyst is
106 difficult. Therefore, developing new catalysts for further decreasing the cost of
107 synthesis, potential secondary pollution, and easy recycle is necessary.

108 Naturally occurring minerals enriched in transition metals may provide an
109 economical alternative for practical water treatment, as which can be readily supplied
110 in large quantities at low cost (Teel et al., 2011; Yan et al., 2015). In this work,
111 natural pyrrhotite (NP, Fe_{1-x}S) is suggested to be a good catalyst to effectively activate
112 PS/PMS for water treatment: the great involvement of Fe^{2+} in NP is beneficial for PS
113 activation and the leached Fe ions are environmental friendly, as well as the specific
114 ferromagnetic properties can facilitate its separation and recycling after utilization
115 (Xia et al., 2015a). In fact, NP is widely dispersed in natural settings and always
116 discarded as a waste due to its over-supply in the sulfuric acid market (Yang et al.,
117 2014). Therefore, it is beneficial to investigate the PS/PMS activation ability of
118 reusing NP waste for both water treatment and mine tailing remediation. Moreover,
119 there still exists contradictory interpretations with respect to the identity of the
120 reactive species and the PS/PMS activation mechanisms (i.e., radical vs non-radical
121 mechanisms, Zhang et al., 2014), which also need to be analyze when NP was
122 involved for PS/PMS activation.

123 In this work, natural pyrrhotite was first utilized to activate PS for *E. coli* K-12
124 inactivation, a model bacterial strains in water (Xia et al., 2015b). To test the activity
125 and applicability of NP/PS system, the inactivation kinetics of *E. coli* K-12 were

126 measured at varying cell density, NP/PS dose, temperature, pH, bicarbonate, authentic
127 wastewater matrix, etc. Meanwhile, its efficiency in terms of radical type and yield, as
128 well as *in situ* ATR-FTIR characterization and chronoamperometric measurements,
129 were collectively applied to analyze the PS activation process occurring on the NP
130 surface. Moreover, microscope was applied to assess damage to cell envelope, and
131 biomolecule assay was utilized to monitor the destruction of cytoplasmic proteins and
132 chromosomal DNA during treatment. Furthermore, the reusability and structural
133 stability of recycled NP were also analyzed. This work may provide a cost-effective
134 method for biohazards inactivation in water-scarce regions, where the wastewater
135 reuse schemes was implemented like agricultural irrigation (Michael-Kordatou et al.,
136 2015 a, b).

137

138 **2. Materials and methods**

139

140 **2.1. Chemicals.** Pristine natural pyrrhotite (NP) mineral was collected from a mining
141 site in Inner Mongolia province, China. Chemical scavengers included methanol
142 (Sigma-Aldrich, USA), tert-butanol alcohol (TBA, Sigma-Aldrich, USA),
143 Fe(II)-EDTA (prepared with FeSO₄ and Na₂EDTA, Ajax Chemicals, Australia) and
144 TEMPOL (Fuchen, China). Sodium persulfate (PS), 5,5-dimethyl-1-pyrrolidine
145 N-oxide (DMPO) were purchased from Aladdin, China. All reagents used were at
146 least analytical grade and prepared in ultrapure water (Millipore, Molsheim France).

147

148 **2.2. Characterization.** The X-ray powder diffraction (XRD) spectra of the NP was
149 recorded on a Bruker D8 Advance X-ray powder diffractometer (Bruker Co., Ltd.).
150 The surface morphology of NP was characterized with a Hitachi S-4800 field

151 emission scanning electron microscope (SEM). The valence states of Fe in NP were
152 examined with an ESCALAB 250XI X-ray photoelectron spectroscopy (XPS,
153 Thermo). The magnetic properties of NP were determined by vibrating sample
154 magnetometer (VSM-7300, Quantum design, Lakeshore, USA) at 25 °C. The in situ
155 ATR-FTIR spectra of the NP was recorded on a Nicolet Fourier transform infrared
156 spectrometer (Magna-IR 750) equipped with a Universal ATR accessory. Purified
157 water was used to identify background noise. The spectra of the NP catalysts were
158 calibrated by subtracting the spectrum of purified water during the scanning processes.
159 Details are listed as follows: First, 50 mg of NP was mixed with 10 mL purified water
160 or PS solution (0.5 mM). After a reaction time of 5 min, the solid particles from the
161 suspensions were scanned in the wavenumber range of 800 to 4000 1/cm at a
162 resolution of 4 1/cm. The leached metal ions were quantified by inductively coupled
163 plasma-optical emission spectrometer (ICP-OES, ULTIMA 2000, HORIDA). The
164 chemical compositions of several randomly selected mineral particles were
165 characterized by electron microprobe analyses (EMPA, JEOL JCXA 733) at China
166 University of Geosciences (Beijing).

167

168 **2.3. Experimental Procedure.** *Escherichia coli* K-12 (Gram -ve, *E. coli* K-12) and
169 *Staphylococcus aureus* (Gram +ve, *S. aureus*) were chosen as model bacterium to
170 evaluate the inactivation ability of NP/PS system. The bacterial cells were cultured in
171 nutrient broth (BioLife, Milano, Italy) at 37 °C with shaking, then harvested in the
172 late exponential phase of growth. The harvested bacteria were centrifuged at 1000
173 rpm for 1 min, and the pellets were resuspended in ultrapure water and recentrifuged
174 at 1000 rpm for 1 min to remove the growth medium, then the final pellets were
175 resuspended in ultrapure water for experiment. A 50 mL suspension including NP of

176 50 mg and *E. coli* K-12 of 2×10^7 cfu (colony forming unit)/mL in a flask was
177 vigorously dispersed by a magnetic stirrer, followed by adding PS (0 to 2 mM) to start
178 the reaction. Aliquot samples were collected at different time intervals and diluted
179 serially with sterilized saline solution, then immediately spread on the nutrient agar
180 (Lab M, Lancashire, UK) plate. All the plates were incubated at 37 °C for 24 h.
181 Control experiments with NP or PS alone were also conducted in triplicate, and the
182 detection limit of spread plate was 1 cfu/mL. To analyze the influence of pH,
183 appropriate amounts of H₂SO₄ (0.1 M) or NaOH (0.1 M) was added to adjust the
184 initial pH. Bacterial inactivation was also conducted in authentic water matrix,
185 including surface water and effluents of secondary wastewater, the detailed water
186 parameters were shown in Table S1 (Supporting Information). Prior to use, the water
187 samples were filtered by glass fiber filters.

188
189 **2.4. Analyses.** (i) Electron paramagnetic resonance (EPR) analysis: A solution
190 containing 10 mM DMPO, 0.5 mM PS was prepared, and then 50 mg NP was added
191 to initiate the reaction. After 0, 5, 10 min of reaction, samples were taken and
192 analyzed on a JEOL FA200 EPR spectrometer; (ii) $\bullet\text{O}_2^-$ was quantitatively analyzed
193 by detecting the decrease in the concentration of nitro blue tetrazolium (NBT, $k = 5.88$
194 $\times 10^4 \text{ M}^{-1} \text{ s}^{-1}$) at a wavelength of 259 nm with a UV-vis spectrophotometer
195 (LabTech); (iii) H₂O₂ was analyzed on a Hitachi F-4500 fluorescence
196 spectrophotometer based on the reaction of H₂O₂ with coumarin to form a high
197 fluorescent compound (7-hydroxycoumarin, 456 nm); (iv) Cell viability assay: *E. coli*
198 K-12 cells treated at various times were tested using a LIVE/DEAD[®]BacLight
199 Bacterial Viability Kit (Molecular Probes, USA) with a fluorescence microscope; (v)
200 Determination of cellular ATP levels: *E. coli* K-12 cells treated at various times were

201 assayed for adenosine triphosphate (ATP) by a luciferin/luciferase test (Bac-Titer-Glo
202 Microbial Cell Viability Assay Kit, Promega), and the luminescence signals were
203 measured in a microplate reader (Biotek Synergy 2); (vi) Leakage of cytoplasmic
204 contents: The residual protein concentration in the captured sample can be measured
205 with the Bradford assay (SK3041, Sangon Biotech, China); Chromosomal DNA was
206 extracted using an Ezup Column Bacteria Genomic DNA Purification Kit (SK8255,
207 Sangon Biotech), then verified by DNA agarose gel electrophoresis (0.6% agarose gel
208 at 100 V for 30 min in $1 \times$ TAE buffer); (vii) Concentration of persulfate was
209 determined using a UV-Vis spectrophotometer (Lambda 25, Perkin Elmer Inc., USA)
210 with a cuvette providing a light path of 10 mm. At each time interval, 1 mL sample
211 was transferred to a 10 mL glass vial containing 9 mL distilled water, followed by
212 adding 0.05 g NaHCO_3 and 1 g KI powder (Liang et al., 2008). The mixture was then
213 hand shaken and set for equilibrium for 15 min before measuring the absorbance at
214 400 nm. The concentration of persulfate was calculated according to the calibration
215 curve.

216

217 **2.5. Chronoamperometry.** NP (5 mg) were first dispersed in 20 μL of nafion
218 perfluorinated resin solution (5 wt %, Aldrich) and 50 mL ethanol (99.9%, Aldrich).
219 The mixture (5 μL) was dropped onto a ITO electrode and dried for 10 min; this
220 procedure was repeated three times. The reactor contained a glassy carbon electrode, a
221 coiled Pt wire, and a Ag/AgCl/KCl (sat) electrode as a working, counter, and
222 reference electrode, respectively and 0.1 M phosphate buffer ($\text{pH} \approx 7$) as an
223 electrolyte. Chronoamperometries were carried out with an open circuit, and
224 electrochemical measurements were subsequently added into the electrochemical
225 working station at stated intervals with final concentrations of 0.5 mM PS and $7 \log_{10}$

226 cfu/mL *E. coli* K-12 cells, respectively.

227

228 3. Results and Discussions

229

230 3.1. Characterization of natural pyrrhotite

231 XRD pattern in Fig. 1a indicates the pristine natural pyrrhotite (NP) is composed
232 of mixed phases of pyrrhotite-6T (Fe_{1-x}S , PDF 29-0725) and pyrite (FeS_2 , PDF
233 42-1340) (Xia et al., 2015a), as NP always occurs with impurity mineral phases. SEM
234 image in Fig. 1b indicates NP powders are in a heterogeneous size ranged from 10 to
235 30 μm and many mechanically ground fractures are observed on NP surface. The
236 surface elements of NP were also analyzed by SEM-EDX (inset of Fig. 1b) and XPS
237 (Fig. 1c). Both results confirmed the main existence of Fe, S and O of NP, and the
238 estimated chemical formula of NP can be expressed as $\text{FeS}_{0.6}\text{O}_{0.52}$. The
239 nonstoichiometric Fe to S ratio revealed vacancies were at the S sites in the crystal
240 structure, mainly due to the oxidation of NP surface. Importantly, the 53.2% of Fe(II)
241 on pristine NP surface (Fig. 1c) indicates its great potential for catalyzing PS to
242 generate reactive species. Apart from Fe and S, Si, Al, K, Ca, Mg, Zn are also existed,
243 based on the results of EMPA in Table S2. As shown in Fig. 1d, the magnetic loop
244 indicates pristine NP possesses a saturation magnetization of 6 emu/g, with little
245 coercivity (16 Oe) and remanence (0.056 emu/g). The soft magnetic property
246 indicates NP can be magnetically recycling without great aggregation (Xia et al.,
247 2016b). As shown in Fig. S1, the NP powders can be immediately drawn to one side
248 of the beaker when an external magnet was placed nearby, indicating its great
249 potential for application.

250

251 3.2. *E. coli* inactivation by NP/PS system

252

253 3.2.1 Reactivity of natural pyrrhotite

254 The adsorption and inactivation profiles of *E. coli* K-12 against the reaction time
255 in various situations are shown in Fig. 2a. The NP alone had no obvious adsorption
256 toward *E. coli* K-12, as no cells' loss occurred within 30 min. Meanwhile, less than
257 0.2 log₁₀ cfu/mL of cells' loss was noticed with PS alone, suggesting that the
258 production of oxidizing radicals from PS alone was limited within 30 min.
259 Impressively, a rapid decrease of the *E. coli* K-12 concentration was observed once
260 the NP was involved, which exhibited a pseudo-first-order kinetics over exposure
261 time with a rate constant of 0.34 1/min. Similarly, the Gram-positive bacteria of *S.*
262 *aureus* with thicker cell envelope was found to exhibit similar inactivation kinetics
263 with *E. coli* K-12 (Ng et al., 2016). This result evidenced that the combination of NP
264 with PS can efficiently inactivate both types of cells.

265 In contrast with NP, the synthesized ZVI of nano-size was also utilized to
266 catalyze PS for *E. coli* inactivation. Attributed to its large specific area, ZVI exhibited
267 a better performance than NP, which can totally inactivate 7 log₁₀ cfu/mL of *E. coli*
268 within 15 min (0.44 1/min, Fig. 2a). The results indicate the catalytic activity of NP is
269 still not comparable with commercial ZVI. However, NP may still can work as an
270 alternative material for PS activation, attributed to its merits like earth abundant and
271 well enough catalytic activity.

272 To further evaluate the catalytic activity from leached ions of NP, the ions

273 leaching in the NP/PS system was also monitored (Fig. S2). In the NP solution, which
274 releases Fe^{2+} slowly and the observed aqueous concentration of total dissolved iron
275 (9.96 mg/L) is comparable to the Fe^{2+} concentration (9.66 mg/L). In the NP/PS
276 system, the total dissolved iron concentration gradually increases to 4.99 mg/L while
277 Fe^{2+} are maintained at relatively low concentrations (0.4 mg/L). This suggests that the
278 released Fe^{2+} could react with PS instantly and form Fe^{3+} . Notably, due to the fact that
279 some of the Fe^{3+} could form $\text{Fe}(\text{OH})_2$ or $\text{Fe}(\text{OH})_3$ and precipitate, thereby the
280 concentration of total soluble Fe amount was halved in the presence of PS. Similar
281 observation was also obtained in other study (Liang et al. 2010). It would be
282 worthwhile observing that leached Fe (especially Fe^{2+}) might be problematic for some
283 applications like wastewater treatment. Therefore, a further precipitation step may be
284 needed to eliminate the dissolved Fe, which can be obtained by the addition of base
285 like NaOH to form $\text{Fe}(\text{OH})_3$. Meanwhile, equivalent amount of leaked Fe^{2+} (10 mg/L)
286 or Fe^{3+} (10 mg/L) was respectively added to catalyze PS for *E. coli K-12* inactivation.
287 As shown in Fig. 2a, due to the low concentration of Fe^{2+} , the Fe^{2+} was consumed
288 quickly and can't trigger enough ROS to attack *E. coli*, thereby only a slight decrease
289 of cell density was noticed. This result also suggests that the bacterial inactivation due
290 to the Fe^{2+} ion-leaching induced homogeneous catalytic reactions was negligible
291 when NP was used as catalysts.

292 The decomposition of PS by NP was also studied through measuring the residual
293 persulfate anion ($\text{S}_2\text{O}_8^{2-}$). The added PS (0.5 mg/L) was sharply decomposed (60%) in
294 the presence of NP, which followed a first-order kinetics' model ($k = 0.021$ 1/min, Fig.
295 2b). Moreover, a notable observation was that the PS decay by NP was further

296 enhanced by *E. coli*, indicating *E. coli* can accelerate the PS activation by NP. In
297 contrast, no noticeable PS decomposition occurred when only *E. coli* added under the
298 same conditions. Thus, it is concluded that the NP is efficient to activate the PS for
299 inactivating *E. coli*.

300

301 3.2.2. Effect of initial NP, *E. coli* K-12 and PS concentration

302 First, *E. coli* K-12 inactivation was carried out to explore the effects of NP
303 loading in the NP/PS system (Fig. 2c). An increase in NP loading had an obvious
304 positive effect on *E. coli* inactivation when NP loading increased from 0.25 g/L to 1
305 g/L, with k value increased from 0.21 1/min to 0.34 1/min, respectively. When NP
306 loading further increased to 1.25 g/L, a slight decline (0.32 1/min) in the *E. coli*
307 inactivation efficiency was noticed, suggesting that the NP dose was the controlling
308 factor of radicals' generation. This inhibition effect at 1.25 g/L of NP can be related to
309 the scavenging effect of the NP, because radicals ($\bullet\text{SO}_4^-$) would be mainly generated
310 by NP activation but they can also react with surface $\equiv\text{Fe(II)}$ on NP in a
311 heterogeneous system. Similar results were also obtained in other work (Yan et al.,
312 2011; Guan et al., 2013).

313 Insignificant difference in inactivation kinetics was observed for different initial
314 *E. coli* K-12 concentrations ranging from 5 to 8 \log_{10} cfu/mL (Fig. 2d), and the
315 measured k value from three batch experiments can be described reasonably well by a
316 similar k value (0.36, 0.34, 0.35 1/min, one way ANOVA, $p > 0.05$). The observed
317 insensitivity to initial cell density is consistent with other disinfection processes like
318 chlorine or ferrate (Luh et al., 2007; Hu et al., 2012).

319 Fig. 2e presents the inactivation efficiencies of *E. coli* K-12 at a varying dosage
320 of PS. The *E. coli* K-12 removal was enhanced with the PS concentration increased

321 from 0.25 mM (0.12 1/min) to 1 mM (0.47 1/min), respectively. This increased
322 inactivation efficiency was mainly resulted from the accelerated generation of radicals
323 that occurred with higher doses of PS. Further increasing the PS concentration to 2
324 mM (0.36 1/min) did not enhance the inactivation efficiency but resulted in a slight
325 inhibition, perhaps due to the quenching of $\bullet\text{SO}_4^-$ by surface Fe(II) of NP (Guan et al.,
326 2013).

327

328 3.3. Reactive species and possible mechanism

329 Obviously, the good *E. coli* inactivation performance of NP/PS system was
330 mainly attributed to the NP activated PS and its great generation of various reactive
331 species. To analyze the presence and contributions of the specific reactive species, *E.*
332 *coli* inactivation performance was thus examined by adding various scavengers in the
333 NP/PS system, including methanol for $\bullet\text{SO}_4^-$, tert-butyl alcohol (TBA) for $\bullet\text{OH}$,
334 Fe(II)-EDTA for H_2O_2 , TEMPOL for $\bullet\text{O}_2^-$ (Xia et al., 2013; Liu et al., 2014). In the
335 control experiment without PS, no significant cells' loss was observed by adding 2
336 mM of each scavenger, indicating no toxicity of these chemical scavengers to the *E.*
337 *coli* within test time period (Fig. S3). First, the inhibition of *E. coli* K-12 inactivation
338 was not accompanied by adding 2 mM TEMPOL, indicating the weak bactericidal
339 contribution of $\bullet\text{O}_2^-$ (Fig. 3a). This is mainly due to the limited formation of $\bullet\text{O}_2^-$ in the
340 NP/PS system, consistent with the result in Fig. S4a. Although O_2 is known to readily
341 accept electron from transition metal to produce $\bullet\text{O}_2^-$, which is unstable and may
342 readily converse into H_2O_2 or $\bullet\text{SO}_4^-$, thereby limited detection occurs in the present
343 condition (Zhang et al., 2017). Second, the involvement of H_2O_2 was affirmed by the
344 moderate decrease in the inactivation kinetics after adding 2 mM Fe(II)-EDTA (1.9
345 \log_{10} cfu/mL of cells survived, Fig. 3a). Generally, when Fe_{1-x}S is exposed to the air,

346 H₂O₂ can be thermodynamically generated by either two electron reduction of
347 surface-adsorbed O₂ from Fe(II) or disproportionate reaction of two •OH (Liu et al.
348 2015; Fang et al., 2016). As show Fig. S4b, the great generation of H₂O₂ was
349 accumulated to almost 5 μM without O₂ purging. Third, methanol and TBA were used
350 to differentiate •SO₄⁻ from •OH, because TBA without an alpha hydrogen was also
351 readily reactive toward •OH, but their reaction with •SO₄⁻ was over 1000-fold slower
352 than methanol (Gao et al., 2016). Obviously, •SO₄⁻ played the leading role rather than
353 •OH was virtually observed, based on the more remarkable inhibition when 2 mM
354 methanol added (5.5 log₁₀ cfu/mL of cells survived, Fig. 3a) than that of 2 mM TBA
355 (3.2 log₁₀ cfu/mL of cells survived, Fig. 3a). Therefore, it can infer that •SO₄⁻ is
356 mainly responsible for bacterial inactivation in the NP/PS system. Moreover, EPR
357 results in Fig. 3b shows the obvious signals of both DMPO-•OH (1:2:2:1) and
358 DMPO-•SO₄⁻ (1:1:1:1:1:1), indicating large quantities of both •OH and •SO₄⁻ radicals
359 were generated immediately in the NP/PS system (Xiong et al., 2014). As identified
360 above, all of the extracellular radicals •SO₄⁻, •OH and H₂O₂ work collectively for the
361 inactivation of *E. coli* K-12.

362 To analyze the interaction occurred on NP surface of NP/PS system, the *in situ*
363 ATR-FTIR characterization was conducted and results were shown in Fig. 3c. After
364 addition of PS, the FTIR spectrum of pristine NP showed an increased absorption at
365 around 1273 1/min and 1046 1/min (the symmetric and asymmetric vibrations of
366 S=O=S of sulfonate group), indicating the adsorptive interaction of PS occurred on
367 NP surface (Lee et al. 2016). Meanwhile, the small band occurred at 1057 1/cm of
368 pristine NP was blue shifted to 1079 1/cm after PS addition, suggesting the formation
369 of a complex at NP surface. It is thus inferred that the interaction between Fe(II) and
370 PS leads to the formation of a weak bond at the surface of NP like

371 $\equiv\text{Fe(II)}\cdots\text{O}_3\text{SO-OSO}_3$ (eq 1), based on Lei et al.'s work (2015). The weak bond of
 372 $\equiv\text{Fe(II)}\cdots\text{O}_3\text{SO-OSO}_3$ could trigger the broken of O-O bond, accompanied by the
 373 generation of $\equiv\text{Fe(III)}$ and $\bullet\text{SO}_4^-$ (eq 2) (Duan et al., 2015, 2016). Meanwhile, the NP
 374 surface $\text{H}_2\text{O}/\text{-OH}$ bond at 3100 $1/\text{cm}$ became relatively invisible after PS addition,
 375 suggesting the complex and generated $\bullet\text{SO}_4^-$ may promote absorbed $\text{H}_2\text{O}/\text{-OH}$ to
 376 transform into $\bullet\text{OH}$ through eq 3, because $\bullet\text{SO}_4^-$ possesses higher oxidative potential
 377 (2.5–3.1 V) than $\bullet\text{OH}$ (Gao et al., 2016). This was confirmed by the observation in
 378 Fig. 3b, the $\text{DMPO}\cdots\text{SO}_4^-$ signals diminished a little, accompanied by a slight increase
 379 in the $\text{DMPO}\cdots\text{OH}$ signals from 1 min to 5 min in NP/PS system, indicating the
 380 $\text{DMPO}\cdots\text{SO}_4^-$ adduct can converse into $\text{DMPO}\cdots\text{OH}$ adduct over time (Zhong et al.,
 381 2015). Subsequently, $\bullet\text{OH}$ may also thermodynamically form into H_2O_2 through
 382 disproportionated reaction (eq 4) (Avetta, et al., 2015; Liu et al., 2015).

383



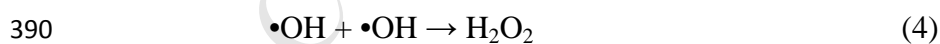
385



387



389



391

392 To further analyze the complex and electron transfer, the current change toward
 393 the NP electrode was detected in the chronoamperometric measurements when PS and
 394 *E. coli* K-12 were added in turn (Fig. 3d). After the injection of PS, a small negative
 395 current peak was detected due to the instant electron movement from the NP electrode

396 to PS, most likely through the formation of charge transfer complex
397 ($\equiv\text{Fe(II)}\cdots\text{O}_3\text{SO-OSO}_3^-$). Subsequently, upon the addition of *E. coli* K-12, a slight
398 positive current flow forms indicated electrons were transferred from *E. coli* K-12 to
399 the NP/PS complex, likely due to the oxidation of bacterial cells occurred. In contrast,
400 no current change occurred when *E. coli* K-12 was directly added on NP (Fig. S5),
401 suggesting no electron transfer reaction happened without PS. Therefore, the PS
402 activation by NP involved electron transfer from NP to PS, and *E. coli* inactivation
403 involved electron transfer from *E. coli* to NP/PS complex, in which NP/PS complex
404 engagement as a facile electron mediation was essential.

405

406 **3.4. Influences of several factors to NP/PS system**

407

408 **3.4.1. Effect of temperature, pH, dissolved oxygen**

409 Reaction temperature is a key operating factor in AOPs. Generally, increasing
410 temperature can accelerate the decomposition rate of PS, thus increase the
411 concentration of $\bullet\text{SO}_4^-$, which also in turn facilitates the AOP reaction (Ji et al., 2015).
412 Therefore, *E. coli* inactivation was examined within a temperature range of 20 °C to
413 50 °C in NP/PS system. First, the results of control experiment at different
414 temperature in Fig. S6a exhibited negligible loss of cells within 30 min, indicating the
415 contribution to cells' loss from thermal activation of PS is limited within this time
416 period. Although the thermal activation of PS to generate sulfate radicals was really
417 occurred at higher temperature like 50 °C (Ji et al., 2015, 2016), some injured cells
418 still can survive after cultivation because of the limited reaction time, thereby no
419 significant loss of *E. coli* density can be observed. In fact, elevated temperature may
420 still favor oxidative reactions based on thermodynamic law. As shown in Fig. 4a, the

421 inactivation kinetics in NP/PS system are similar with the general trend, indicating
422 higher temperature resulting in higher inactivation efficiency. The measured rate
423 constant increased roughly 2-fold when temperature was increased from 20 °C (0.34
424 1/min) to 50 °C (0.69 1/min). On the basis of this trend, it might be deduced that PS
425 activation process by NP is endothermic: higher temperature would shift the
426 equilibrium to produce more reactive species and thus improve the bacterial
427 inactivation efficiency (Feng et al. 2016).

428 Inactivation kinetics (Fig. 4b) in NP/PS system was found to be highly dependent
429 on pH, lower pH can obtain a higher inactivation performance. The control
430 experiments with PS alone at different pH was also conducted, and no significant *E.*
431 *coli*' loss occurred within 20 min, indicating the pH has no obvious effect on cells'
432 viability (Fig. S6b). In general, $\bullet\text{SO}_4^-$ based AOP can achieve a higher oxidative
433 activity at higher pH, due to the $\bullet\text{SO}_4^-$ could provoke an accelerated PS decomposition
434 and transformation reactions generating additional $\bullet\text{OH}$ under alkaline condition (Lei
435 et al., 2015; Neta et al., 1988). However, PS solution with a pH 3.0 (0.68 1/min)
436 demonstrated the best inactivation performance, and a >1.5-fold decline was observed
437 at pH 5.0 (0.45 1/min). When pH was increased from 7 (0.30 1/min) to 9 (0.17 1/min),
438 the inactivation kinetics were observed to decrease roughly 1.7-fold. To analyze the
439 pH effect, the surface charge of NP and *E. coli* have been detected at different pH
440 conditions. As shown in Fig. S7, the zero charge of NP is 4.6, while *E. coli* exists
441 predominantly in its deprotonated form at pH 3.0-11.0. Therefore, the high
442 inactivation efficiency at acidic condition (pH 3, 5) can be attributed to the
443 electrostatic adsorption, while the low inactivation at pH 9, 11 was probably in part
444 due to the electrostatic repulsion between the deprotonated *E. coli* and NP, because
445 almost all of the cells had a negative charge under such conditions (Fig. S7).

446 Moreover, at alkaline condition, the oxidized Fe^{3+} ions may form oxyhydroxides like
447 $\text{FeOH}^{2+}/\text{Fe}_2(\text{OH})_2^+/\text{Fe}(\text{OH})_3$ to precipitate on the surface of NP, which covered the
448 surface reactive sites of NP and caused inhibition for activating PS to form $\bullet\text{SO}_4^-$
449 (Zhang et al., 2017). Notably, the pH variation in NP/PS system was also monitored at
450 five initial pH, all the pH values were decreased a little and rapidly to a specific pH
451 value (Fig. S8), this is mainly due to the partial dissolution of Fe_{1-x}S in the water (Liu
452 et al., 2015). Since the pH was rapidly attained to an equilibrium, and no significant
453 cells' loss was observed with NP alone/PS alone and even in the pH controlled
454 solution, it is reasonable to indicate that the *E. coli* inactivation by dissolved NP
455 induced pH interference may not that significant. Therefore, the inactivation kinetics
456 revealed that the bacterial inactivation process was more favorable in acidic and mild
457 alkaline conditions.

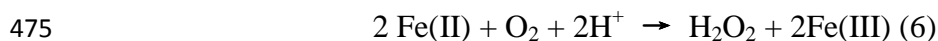
458 Dissolved O_2 has an impact on PS activation as O_2 is an electron acceptor. As
459 shown in Fig. 4c, the total inactivation of $7 \log_{10}$ cfu/mL of *E. coli* was obtained at 15
460 min with air purging (0.46 1/min) and 20 min without air purging (0.34 1/min), while
461 only $4.6 \log_{10}$ cfu/mL of *E. coli* was obtained at 20 min under N_2 purging (0.23 1/min).
462 When Fe(II) is exposed to the air, molecular O_2 could be reduced to $\bullet\text{O}_2^-$ or H_2O_2
463 directly by Fe(II) via single- or two-electron transfer routes (Harrington et al., 2012;
464 Jones et al. 2013), which would accelerate the PS activation to produce $\bullet\text{SO}_4^-$ (Zhang
465 et al., 2017) (eqs. 5-8). To test the effects of dissolved O_2 , the generated $\bullet\text{O}_2^-$ and
466 H_2O_2 concentrations were determined. Results in Fig. S4a present the little formation
467 of $\bullet\text{O}_2^-$ (no NBT transformation occurred at three conditions), while H_2O_2
468 concentration increased in the order of N_2 purging-pyrite system ($3 \mu\text{M}$) > no purging
469 pyrite system ($4.995 \mu\text{M}$) > air purging-pyrite system ($5.65 \mu\text{M}$) (Fig. S4b). Therefore,
470 increasing O_2 concentration could lead to the generation of more H_2O_2 , thus to trigger

471 more generation of $\bullet\text{SO}_4^-$, collectively resulting in a higher inactivation efficiency.

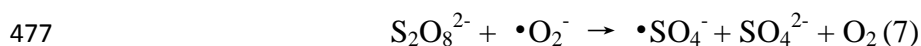
472



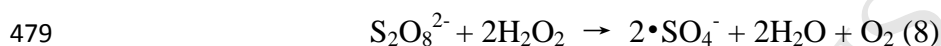
474



476



478



480

481 3.4.2. Effect of bicarbonate, NOM.

482 Bicarbonate was the representative of inorganic carbon existed in natural water at
483 the range of 0.1 to 50 mg/L, which can quench radicals to inhibit oxidation process
484 (Wu et al., 2015). As shown in Fig. 4d, a NaHCO_3 concentration to 1 mg/L (0.34
485 1/min) exhibited similar inactivation kinetics with that of no NaHCO_3 addition (0.34
486 1/min); with further addition of NaHCO_3 , the inactivation efficiency decreased
487 significantly (one way ANOVA, $p < 0.05$) in the presence of 5 mg/L NaHCO_3 (0.29
488 1/min) and almost totally inhibited when 20 mg/L NaHCO_3 (0.055 1/min) were added.
489 Wu et al. (2015) suggested that bicarbonate could form complexes on catalyst surface
490 and even quench the $\bullet\text{SO}_4^{2-}$ to generate the $\bullet\text{CO}_3^-$. The great consumption of $\bullet\text{SO}_4^{2-}$
491 and the relative lower reactivity of $\bullet\text{CO}_3^-$ (2.09 eV) than $\bullet\text{SO}_4^{2-}$ (2.5-3.1 eV, Zhao et
492 al., 2010) would cause the detrimental effect to NP/PS system, thus to greatly inhibit
493 *E. coli* K-12 inactivation.

494 Similarly, natural organic matter (NOM) is usually present in the aquatic
495 environment, which can act as radical scavenger via competing for $\bullet\text{OH}$ and $\bullet\text{SO}_4^-$. As

496 shown in Fig. 4e, *E. coli* inactivation rate was firstly promoted to 0.36 1/min with the
497 addition of 1 mg/L NOM, in contrast with free NOM (0.34 1/min). In fact,
498 hydroquinones, quinones and phenols in NOM can form into semiquinone radicals,
499 which might stimulate the decomposition of PS into $\bullet\text{OH}$ and $\bullet\text{SO}_4^-$, similar to the
500 way of reducing H_2O_2 to $\bullet\text{OH}$, thus to accelerate the AOP process (De Laat et al.,
501 2011). However, the *E. coli* inactivation rate then decreased significantly from 0.23
502 1/min to 0.055 1/min when NOM further increased from 5 mg/L to 20 mg/L,
503 indicating the stimulated effect of NOM was overwhelmed by its detrimental effect.
504 Michael-Kordatou et al. (2015b) suggested that NOM contains many phenolic
505 hydroxyl and carboxyl groups, which can be adsorbed onto catalyst surface and block
506 reactive sites, thus to inhibit the oxidation process.

507

508 3.5. Cell destruction process

509 The bacterial envelope, composed of outer membrane, peptidoglycan layer, and
510 cytoplasmic membrane, always worked as the first target of being exposed to ROS
511 attack (Xia et al., 2016a). First, the BacLight kit fluorescent microscopic method was
512 utilized to directly observe the permeability changes of cell envelop in the NP/PS
513 system. As shown in Fig. 5a, the viable cells were with intense green fluorescence.
514 After being treated for 10 min, most cells turned to red fluorescence, indicating most
515 cells were disrupted and intracellular components were stained. With prolonged
516 treatment to 20 min, all the images were in red, indicating cells' envelope were all
517 broken with more red stained intracellular components. Similarly, compared with the
518 SEM image of initial intact *E. coli* K-12 cells (0 min) in Fig. 5b, the treated cell
519 envelope was deformed after 20 min treatment. Actually, the cell envelope contains
520 essential protein components such as respiratory chain, which generate energy (ATP)

521 with functionalized electron chains, playing a vital role in bacterial metabolism
522 (Bosshard et al., 2010). Associated with the damaged envelope, the cells were almost
523 instantaneously inactivated by metabolic arrest as a consequence of a drastic drop in
524 the ATP level within initial 10 min treatment (Fig. 5c). Generally, ROS has been
525 found to inhibit ATP formation either by behaving like a protonophore or by
526 inhibiting enzymes in the respiratory chain to dissipate the proton motive force (Park
527 et al. 2009).

528 After the penetration of cell envelope, the ROS can subsequently injure the cells
529 by reacting with various biomolecules, such as cytoplasmic protein and genome (Sun
530 et al., 2014). As shown in Fig. 5d, the protein content of treated cells (10 mL) in
531 Bradford assay was maintained at around 142 mg/mL within the initial 10 min but
532 then decreased a little to 136.7 mg/mL at 20 min, assumed to be indicative of starting
533 peroxidation of protein during treatment. The destruction of genomic DNA could be
534 observed in Fig. 5e because the fluorescent intensity of the DNA bands started to fade
535 around 20 min and then totally disappeared with prolonged to 1 h. Damage to *E.*
536 *coli*'s genome is lethal to the cells, which could efficiently disrupt events instrumental
537 to the bacterial life cycle. Or else cells in a viable but non-culturable state may still
538 survive to cause the health risks in water (Zhang et al., 2015). These results revealed
539 that the cell envelope of *E. coli* K-12 was firstly decomposed, then cytoplasmic
540 components leaked and degraded, finally resulting in the cells' mineralization.

541

542 **3.6. Stability and recycle of NP**

543 The stability of NP was investigated by repeating *E. coli* inactivation experiments
544 with recycled NP. After each experiment, NP was magnetically captured on the
545 bottom of flask and the supernatant was poured out, then *E. coli* K-12 cells and PS

546 solution were added to start the next run. After four times' recycling, the *E. coli* K-12
547 inactivation efficiency decreased with about 4 log₁₀ cfu/mL cells' inactivation (Fig.
548 6a), which was likely due to the loss of active sites on the NP surfaces, including
549 oxidation of surface Fe(II) and adsorption of *E. coli* oxidation products. XPS results
550 (Fig. 1c) confirmed that the atomic ratio of ≡Fe(II)/≡Fe(III) was decreased from 1.14
551 (53.2%/46.8%) for pristine NP to 0.93 (48.1%/51.9%) for used NP, thus resulting in a
552 decreased performance. Meanwhile, FTIR analysis (Fig. S9) also show that
553 out-of-plane was bend of amide A (3274 1/min) and amide B (3060 1/min) groups of
554 *E. coli* after treatment, which inhibit the surface Fe(II) to contact with PS (Xia et al.,
555 2013). The semi-quantitative analysis of XRD pattern (Fig. 1a) showed that the ratio
556 of py/ph decreased from 745/370 (2.01) to 405/318 (1.27), which may suggest the
557 partial crystalline change from py to ph after reaction. However, no significant
558 difference was observed in the saturated magnetism between fresh and recycled NP
559 (Fig. 1a, d), indicating the magnetism of NP were still maintained even after 4 runs'
560 test. After the fourth run, the recovered NP was washed by ultrapure water and dried
561 for the fifth run. The *E. coli* inactivation efficiency almost recovered to that of initial
562 run (Fig. 6a). This is mainly due to the cellular debris were removed from NP after
563 wash treatment, as the characteristic peaks of organic functional groups greatly
564 weakened (Fig. S9).

565

566 **3.7. Environmental implications for authentic water treatments.**

567 As a preliminary step in investigating the potential application of NP/PS system,
568 the inactivation experiments were thus conducted under authentic matrices of surface
569 water (SW) and secondary wastewater effluents (WW). In contrast with that of
570 ultrapure water (UPW), the inactivation kinetics in SW and WW decreased

571 significantly, with the order of: UPW > SW > WW (Fig. S10). Based on the water
572 parameters in Table. S1, it can conclude that the slowed performances in SW and
573 WW, were mainly caused by the natural water components like natural organic matter
574 (TOC represents NOM) and inorganic ions (bicarbonate). $\bullet\text{SO}_4^-$ can react selectively
575 against the prevailed nitrogen-containing organics in NOM through an electron
576 transfer oxidation mechanism, thus the SW (TOC = 0.72 mg C/L) and WW (TOC =
577 5.4 mg C/L) are suspected to have a high $\bullet\text{SO}_4^-$ reactivity hindering the bacterial
578 inactivation (Avetta, et al., 2015). Meanwhile, part of $\bullet\text{SO}_4^-$ may complex or react
579 with CO_3^{2-} present in the SW (bicarbonate = 6 mg/L) and WW (bicarbonate = 12
580 mg/L), also can greatly inhibit bacterial inactivation (Michael-Kordatou et al., 2015b).
581 Moreover, both water matrices are at alkaline conditions (pH 8.3 of SW and pH 7.64
582 of WW) may also inhibit the inactivation efficiency to some content, based on the
583 study of pH effect in Fig. 4b.

584 When the PS amount increased to 1 mM, NP/PS can totally inactivate the cells
585 within 25 min in SW; while $3.5 \log_{10}$ cfu/mL of *E. coli* still survive within 30 min in
586 WW (Fig. S10). Further increase the PS amount to 2 mM, there are $2 \log_{10}$ cfu/mL of
587 *E. coli* still survive in WW (Fig. S10). Obviously, the inactivation efficiency was
588 greatly enhanced with the increase amount of PS in both water matrices. The higher
589 the concentration of PS, the more PS anions can be activated by NP, together with
590 more sulfate radicals and derived ROS to inactivate cells (Feng et al., 2016). Based on
591 the results, the selected suitable amount of PS was 1 mM for SW and 2 mM for WW,
592 respectively.

593 In contrast, ZVI was also utilized to activate the selected amount of PS for *E. coli*
594 inactivation, which exhibiting a slightly higher performance than that of NP/PS
595 system in both UPW and authentic water matrices (Fig. 6b). This is probably occurred,

596 because ZVI can accelerate the Fe(III)-Fe(II) cycle, thus to accelerate the PS
597 activation (Liang et al., 2010). Meanwhile, ZVI also can react with dissolved oxygen
598 to generate $\bullet\text{O}_2^-$ and a series of other ROS to further enhance the inactivation
599 efficiency (Zhong et al., 2015). Although the catalytic activity of NP is still not
600 comparable with commercial ZVI in different water matrices, NP still can be utilized
601 as a cost-effective alternative material for application, attributed to its merits like
602 earth abundant, good catalytic activity, and easy recyclable. In the framework of
603 implementing safe wastewater reuse schemes, other technological parameters like
604 reactor size, stirring velocity, etc., should be further optimized to meet the current
605 challenges associated with hazardous bacteria spread into the environment.

606

607 **4. Conclusions**

608 Natural occurring pyrrhotite exhibited a notable catalytic activity to PS for *E. coli*
609 inactivation. *E. coli* inactivation by NP/PS was enhanced with the increase of PS and
610 NP doses at respective range of 0.2-1.0 mM and 0.15-1.0 g/L. It showed an
611 independence on initial cell density, but greatly dependent on acidic pH and dissolved
612 O_2 . NOM stimulated *E. coli* inactivation at the concentration of 1 mM but inhibited at
613 5-20 mg/L. Bicarbonate inhibited the *E. coli* inactivation at the range of 0.1-2.0 mg/L.
614 The bactericidal role of generated ROS was identified to be $\bullet\text{SO}_4^- > \bullet\text{OH} > \text{H}_2\text{O}_2$. The
615 surface complex of NP played an important role in the generation of radicals from
616 NP/PS. Catalytic oxidation of *E. coli* by NP/PS was also effective under the
617 backgrounds of investigated actual waters, which provide a reference for application.

618

619 Acknowledgement

620 The project was supported by a research grant (GRF14100115) of the Research
621 Grant Council, Hong Kong SAR Government and the Technology and Business
622 Development Fund (TBF15SCI008) of The Chinese University of Hong Kong to P.K.
623 Wong, and the research grants (41573086, 41425015 and 41603097) of National
624 Science Foundation of China to Dr. G.Y. Li, T.C. An, D.H. Xia, respectively. P.K.
625 Wong was also supported by CAS/SAFEA International Partnership Program for
626 Creative Research Teams of Chinese Academy of Sciences.

627 The Supporting Information included the authentic water parameters, iron
628 leakage, FTIR of used NP, Chronoamperometric measurements of NP electrode.

629

630 References

631

632 Ahn, S., Peterson, T. D., Righter, J., Miles, D. M., Tratnyek, P. G., 2013. Disinfection
633 of ballast water with iron activated persulfate. *Environ. Sci. Technol.* 47,
634 11717-11725.

635

636 Anastasi, E.M., Wohlsen, T.D., Stratton, H.M., Katouli, M., 2013. Survival of
637 *Escherichia coli* in two sewage treatment plants using UV irradiation and chlorination
638 for disinfection. *Water Res.* 47, 6670-6679.

639

640 Anipsitakis, G. P., Tufano, T. P., Dionysiou, D. D., 2008. Chemical and microbial
641 decontamination of pool water using activated potassium peroxymonosulfate. *Water*
642 *Res.* 42, 2899-2910.

643

- 644 Avetta, P., Pensato, A., Minella, M., Malandrino, M., Maurino, V., Minero, C., Hanna,
645 K., Vione, D., 2015. Activation of persulfate by irradiated magnetite: implications for
646 the degradation of phenol under heterogeneous photo-Fenton-like conditions. *Environ.*
647 *Sci. Technol.* 49, 1043-1050.
- 648
- 649 Bosshard, F., Bucheli, M., Meur, Y., Egli, T., 2010. The respiratory chain is the cell's
650 Achilles' heel during UVA inactivation in *Escherichia coli*. *Microbiology* 156 (7),
651 2006-2015.
- 652
- 653 Chesney, A. R., Booth, C. J., Lietz, C. B., Li, L., Pedersen, J. A. 2016.
654 Peroxymonosulfate rapidly inactivates the disease-associated prion protein. *Environ.*
655 *Sci. Technol.* 50, 7095-7105.
- 656
- 657 De Laat, J., Dao, Y. H., Hamdi El Najjar, N., Daou, C., 2011. Effect of some
658 parameters on the rate of the catalysed decomposition of hydrogen peroxide by
659 iron(III)-nitrilotriacetate in water. *Water Res.* 45 (17), 5654-5664.
- 660
- 661 Dobrowsky, P.H., De Kwaadsteniet, M., Cloete, T.E., Khan, W., 2014. Distribution of
662 indigenous bacterial pathogens and potential pathogens associated with roof harvested
663 rainwater. *Appl. Environ. Microbiol.* 80, 2307-2316.
- 664
- 665 Drzewicz, P., Perez-Estrada, L., Alpatova, A., Martin, J. W., Gamal El-Din, M., 2012.
666 Impact of peroxydisulfate in the presence of zero valent iron on the oxidation of
667 cyclohexanoic acid and naphthenic acids from oil sands process-affected water
668 intermediates and reaction pathways from the degradation of microcystin-LR with

- 669 sulfate radicals. *Environ. Sci. Technol.* 46, 8984-8991.
- 670
- 671 Duan, X., Su, C., Zhou, L., Sun, H., Suvorova, A., Odedairo, T., Zhu, Z., Shao, Z.,
672 Wang, S., 2016. Surface controlled generation of reactive radicals from persulfate by
673 carbocatalysis on nanodiamonds. *Appl. Catal. B: Environ.* 194, 7-15.
- 674
- 675 Duan, X., Sun, H., Kang, J., Wang, Y., Indrawirawan, S., Wang, S., 2015. Insights
676 into heterogeneous catalysis of persulfate activation on dimensional-structured
677 nanocarbons. *ACS Catal.* 5, 4629-4636.
- 678
- 679 Eischeid, A.C., Thurston, J.A., Linden, K.G., 2011. UV disinfection of adenovirus:
680 present state of the research and future directions. *Crit. Rev. Environ. Sci. Technol.* 41,
681 1375-1396.
- 682
- 683 Fang, G.-D., Dionysiou, D. D., Al-Abed, S. R., Zhou, D.-M., 2016. Superoxide
684 radical driving the activation of persulfate by magnetite nanoparticles: implications
685 for the degradation of PCBs. *Appl. Catal. B: Environ.* 194, 7-15.
- 686
- 687 Feng, Y., Wu, D., Deng, Y., Zhang, T., Shih, K. M., 2016. Sulfate radical-mediated
688 degradation of sulfadiazine by CuFeO_2 rhombohedral crystal-catalyzed
689 peroxymonosulfate: synergistic effects and mechanisms. *Environ. Sci. Technol.* 50,
690 3119-3127.
- 691
- 692 Gao, Y., Zhang, Z., Li, S., Liu, J., Yao, L., Li, Y., Zhang, H., 2016. Insights into the
693 mechanism of heterogeneous activation of persulfate with a clay/iron-based catalyst

- 694 under visible LED light irradiation. *Appl. Catal. B: Environ.* 185, 22-30.
- 695
- 696 Guan, Y. H., Ma, J., Li, X. C., Fang, J. Y., Chen, L. W., 2011. Influence of pH on the
697 formation of sulfate and hydroxyl radicals in the UV/peroxymonosulfate system.
698 *Environ. Sci. Technol.* 45, 9308-9314.
- 699
- 700 Guan, Y., Ma, J., Ren, Y., Liu, Y., Xiao, J., Lin, L., Zhang, C., 2013. Efficient
701 degradation of atrazine by magnetic porous copper ferrite catalyzed
702 peroxymonosulfate
703 oxidation via the formation of hydroxyl and sulfate radicals. *Water Res.* 47,
704 5431-5438.
- 705
- 706 Haaken, D., Dittmar, T., Schmalz, V., Worch, E., 2014. Disinfection of biologically
707 treated wastewater and prevention of biofouling by UV/electrolysis hybrid technology:
708 influence factors and limits for domestic wastewater reuse. *Water Res.* 52, 20-28.
- 709
- 710 Harrington, A. D., Hylton, S., Schoonen, M. A. A., 2012. Pyrite-driven reactive
711 Oxygen species formation in simulated lung fluid: implications for coal workers'
712 pneumoconiosis. *Environ. Geochem. Health* 34, 527–538.
- 713
- 714 Hu, L., Page, M. A., Sigstam, T., Kohn, T., Marinas, B. J., Strathmann, T. J., 2012.
715 Inactivation of bacteriophage MS2 with potassium Ferrate(VI). *Environ. Sci. Technol.*
716 46, 12079-12087.
- 717
- 718 Hu, P., Long, M., 2016. Cobalt-catalyzed sulfate radical-based advanced oxidation: A

719 review on heterogeneous catalysts and applications. *Appl. Catal. B: Environ.* 181,
720 103-117.

721

722 Huang, G., Ng, T. W., An, T., Li, G., Xia, D., Yip, H. Y., Zhao, H., Wong, P. K.,
723 2017. Probing the intracellular organic matters released from the photocatalytic
724 inactivation of bacteria using fractionation procedure and excitation-emission-matrix
725 fluorescence. *Water Res.* 110, 270-280.

726

727 Ji, Y., Fan, Y., Liu, K., Kong, D., Lu, J., 2015. Thermo activated persulfate oxidation
728 of antibiotic sulfamethoxazole and structurally related compounds. *Water Res.*, 87,
729 1-9.

730

731 Ji, Y., Shi, Y., Dong, W., Wen, X., Jiang, M., Lu, J., 2016. Thermo-activated
732 persulfate oxidation system for tetracycline antibiotics degradation in aqueous
733 solution. *Chem. Eng. J.*, 298, 225-233.

734

735 Johnson, R. L., Tratnyek, P. G., Johnson, R. O. B., 2008. Persulfate persistence under
736 thermal activation conditions. *Environ. Sci. Technol.* 42, 9350-9356.

737

738 Jones, G. C., van Hille, R. P., Harrison, S. T. L., 2013. Reactive Oxygen Species
739 Generated in the Presence of Fine Pyrite Particles and Its Implication in Thermophilic
740 Mineral Bioleaching. *Appl. Microbiol. Biotechnol.* 97, 2735-2742.

741

742 Lee, H., Kim, H., Weon, S., Choi, W., Hwang, Y. S., Seo, J., Lee, C., Kim, J.-H.,

743 2016. Activation of persulfates by graphitized nanodiamonds for removal of organic
744 compounds. *Environ. Sci. Technol.* 50 (18), 10134-10142.

745

746 Lei, Y., Chen, C.-S., Tu, Y.-J., Huang, Y.-H., Zhang, H., 2015. Heterogeneous
747 degradation of organic pollutants by persulfate activated by CuO-Fe₃O₄: mechanism,
748 stability, and effects of pH and bicarbonate ions. *Environ. Sci. Technol.* 49,
749 6838-6845.

750

751 Liang, C., Guo, Y.Y., Chien, Y. C., Wu, Y.J., 2010. Oxidative degradation of MTBE
752 by pyrite-activated persulfate: proposed reaction pathways. 49, 8858-8864.

753

754 Liang, C., Huang, C.F., Mohanty, N., Kurakalva, R. M., 2008. A rapid
755 spectrophotometric determination of persulfate anion in ISCO. *Chemosphere* 73,
756 1540-1543.

757

758 Liang, C. J. and Guo, Y.Y., 2010. Mass transfer and chemical oxidation of
759 naphthalene particles with zerovalent iron activated persulfate. *Environ. Sci. Technol.*
760 44, 8203-8208.

761

762 Liu, H., Bruton, T. A., Doyle, F. M., Sedlak, D. L., 2014. In situ chemical oxidation
763 of contaminated groundwater by persulfate: decomposition by Fe(III)- and
764 Mn(IV)-containing oxides and aquifer materials. *Environ. Sci. Technol.* 48,
765 10330-10336.

766

767 Liu, W., Wang, Y., Ai, Z., Zhang, L., 2015. Hydrothermal synthesis of FeS₂ as a

768 high-efficiency Fenton reagent to degrade alachlor via superoxide-mediated
769 Fe(II)/Fe(III) cycle. ACS Appl. Mater. Interfaces 7 (51), 28534-28544.

770

771 Luh, J., Marinas, B. J., 2007. Inactivation of *Mycobacterium avium* with free chlorine.
772 Environ. Sci. Technol. 41 (14), 5096-5102.

773

774 Matzek, L.W. and Carter, K.E., 2016. Activated persulfate for organic chemical
775 degradation: a review. Chemosphere 151, 178-188.

776

777 Michael-Kordatou, I., Iacovou, M., Frontistis, Z., Hapeshi, E., Dionysiou, D. D.,
778 Fatta-Kassinos, D., 2015a. Erythromycin oxidation and ERY-resistant *Escherichia*
779 *coli* inactivation in urban wastewater by sulfate radical-based oxidation process under
780 UV-C irradiation. Water Res. 85, 346-358.

781

782 Michael-Kordatou, C., Michael, X., Duan, X., He, D., Dionysiou, M. A., Mills,
783 Fatta-Kassinos, D., 2015b. Effluent organic matter: characteristics and potential
784 implications in wastewater treatment and reuse applications. Water Res. 77, 213-248.

785

786 Neta, P., Huie, R. E., Ross, A. B., 1988. Rate constants for reactions of inorganic
787 radicals in aqueous solution. J. Phys. Chem. Ref. Data 17 (3), 1027-1284.

788

789 Ng, T. W., Zhang, L., Liu, J., Huang, G., Wang, W., Wong, P. K., 2016.
790 Visible-light-driven photocatalytic inactivation of *Escherichia coli* by magnetic
791 Fe₂O₃-AgBr. Water Res. 90, 111-118.

792

793 Oh, W.-D., Dong, Z., Lim, T.-T., 2016. Generation of sulfate radical through
794 heterogeneous catalysis for organic contaminants removal: current development,
795 challenges and prospects. *Appl. Catal. B: Environ.* 194, 169-201.

796

797 Parker, K.M., Zeng, T., Harkness, J., Vengosh, A., Mitch, W.A., 2014. Enhanced
798 formation of disinfection byproducts in shale gas wastewater-impacted drinking water
799 supplies. *Environ. Sci. Technol.* 48, 11161-11169.

800

801 Ren, Y., Lin, L., Ma, J., Yang, J., Feng, J., Fan, Z., 2015. Sulfate radicals induced
802 from peroxymonosulfate by magnetic ferrosphel MFe_2O_4 (M = Co, Cu, Mn and Zn)
803 as heterogeneous catalysts in the water. *Appl. Catal. B: Environ.* 165, 572-578.

804

805 Rietveld, L.C., Norton-Brandao, D., Shang, R., van Agtmaal, J., van Lier, J.B., 2011.
806 Possibilities for reuse of treated domestic wastewater in The Netherlands. *Water Sci.*
807 *Technol.* 64, 1540-1546.

808

809 Rizzo, L., Maniaia, C., Merlin, C., Schwartz, T., Dagot, C., Ploy, M., Michael, I.,
810 Fatta-Kassinos, D., 2013a. Urban wastewater treatment plants as hotspots for
811 antibiotic resistant bacteria and genes spread into the environment: a review. *Sci.*
812 *Total Environ.* 447, 345-360.

813

814 Rizzo, L., Fiorentino, A., Anselmo, A., 2013b. Advanced treatment of urban
815 wastewater by UV radiation: effect on antibiotics and antibiotic-resistant *E. coli*
816 strains. *Chemosphere* 92, 171-176.

817

- 818 Sharma, V.K., Zboril, R., McDonald, T.J., 2014. Formation and toxicity of
819 brominated
820 disinfection byproducts during chlorination and chloramination of water: a review. *J.*
821 *Environ. Sci. Health B* 49, 212-228.
- 822
- 823 Soller, J.A., Schoen, M.E., Varghese, A., Ichida, A.M., Boehm, A.B., Eftim, S.,
824 Ashbolt, N.J., Ravenscroft, J.E., 2014. Human health risk implications of multiple
825 sources of faecal indicator bacteria in a recreational waterbody. *Water Res.* 66,
826 254-264.
- 827
- 828 Sun, H. W., Li, G. Y., Nie, X., Shi, H. X., Wong, P. K., Zhao, H. J., An, T. C., 2014.
829 Systematic approach to in-depth understanding of photoelectrocatalytic bacterial
830 inactivation mechanisms by tracking the decomposed building blocks. *Environ. Sci.*
831 *Technol.* 48, 9412-9419.
- 832
- 833 Teel, A. L., Ahmad, M., Watts, R. J., 2011. Persulfate activation by naturally
834 occurring trace minerals. *J. Hazard. Mater.* 196, 153-159.
- 835
- 836 Tsitonaki, A., Smets, B. F., Bjerg, P. L., 2008. Effects of heat-activated persulfate
837 oxidation on soil microorganisms. *Water Res.* 42, 1013-1022.
- 838
- 839 Waldemer, R. H., Tratnyek, P. G., Johnson, R. L., Nurmi, J. T., 2007. Oxidation of
840 chlorinated ethenes by heat-activated persulfate: kinetics and products. *Environ. Sci.*
841 *Technol.* 41, 1010-1015.
- 842

843 Wang, X., Qin, Y., Zhu, L., Tang, H., 2015. Nitrogen-doped reduced graphene oxide
844 as a bifunctional material for removing bisphenols: synergistic effect between
845 adsorption and catalysis. *Environ. Sci. Technol.* 49, 6855-6864.

846

847 Wang, Y., Sun, H., Ang, H.M., Tade, M.O., Wang, S., 2014. Facile synthesis of
848 hierarchically structured magnetic $\text{MnO}_2/\text{ZnFe}_2\text{O}_4$ hybrid materials and their
849 performance in heterogeneous activation of peroxydisulfate. *ACS Appl. Mater.*
850 *Interf.* 6, 19914-19923.

851

852 Wu, Y., Bianco, A., Brigante, M., Dong, W., Sainte-Claire, P., Hanna, K., Mailhot, G.,
853 2015. Sulfate radical photogeneration using Fe-EDDS: influence of critical
854 parameters and naturally occurring scavengers. *Environ. Sci. Technol.* 49,
855 14343-14349.

856

857 Xia, D., Ng, T. W., An, T., Li, G., Li, Y., Yip, H. Y., Zhao, H., Lu, A., Wong, P. K.,
858 2013. A recyclable mineral catalyst for visible-light-driven photocatalytic inactivation
859 of bacteria: natural magnetic sphalerite. *Environ. Sci. Technol.* 47, 11166-11173.

860

861 Xia, D., Li, Y., Huang, G., Fong, C. C., An, T., Li, G., Yip, H. Y., Zhao, H., Lu, A.,
862 Wong, P. K., 2015a. Visible-light-driven inactivation of *Escherichia coli* K-12 over
863 thermal treated natural pyrrhotite. *Appl. Catal. B: Environ.* 176-177, 749-756.

864

865 Xia, D., Shen, Z., Huang, G., Wang, W., Yu, J., Wong, P. K., 2015b. Red phosphorus:
866 an earth-abundant elemental photocatalyst for "green" bacterial inactivation under
867 visible light. *Environ. Sci. Technol.* 49, 6264-6273.

868

869 Xia, D., An, T., Li, G., Li, Y., Yip, H. Y., Zhao, H., Wong, P. K. 2016a. Synergistic
870 photocatalytic inactivation mechanisms of bacteria by graphene sheets grafted
871 plasmonic Ag-AgX (X = Cl, Br, I) composite photocatalyst under visible light
872 irradiation. *Water Res.* 99, 149-161.

873

874 Xia, D., Lo, I. M. C., 2016b. Synthesis of magnetically separable Bi₂O₄/Fe₃O₄ hybrid
875 nanocomposites with enhanced photocatalytic removal of ibuprofen under visible
876 light irradiation. *Water Res.* 100, 393-404.

877

878 Xiong, X., Sun, B., Zhang, J., Gao, N., Shen, J., Li, J., Guan, X., 2014. Activating
879 persulfate by Fe⁰ coupling with weak magnetic field: performance and mechanism.
880 *Water Res.* 62, 53-62.

881

882 Yan, J.; Lei, M.; Zhu, L.; Anjum, M. N.; Zou, J.; Tang, H., 2011. Degradation of
883 sulfamonomethoxine with Fe₃O₄ magnetic nanoparticles as heterogeneous activator of
884 persulfate. *J. Hazard. Mater.* 186, 1398-1404.

885

886 Yan, N., Liu, F., Xue, Q., Brusseau, M. L., Liu, Y., Wang, J., 2015. Degradation of
887 trichloroethene by siderite-catalyzed hydrogen peroxide and persulfate: investigation
888 of reaction mechanisms and degradation products. *Chem. Eng. J.* 274, 61-68.

889

890 Yang, Z., Kang, M., Ma, B., Xie, J., Chen, F., Charlet, L., Liu, C., 2014. Inhibition of
891 U(VI) reduction by synthetic and natural pyrite. *Environ. Sci. Technol.* 48,
892 10716-10724.

893

894 Yuan, S., Liao, P., Alshawabkeh, A. N., 2014. Electrolytic manipulation of persulfate
895 reactivity by iron electrodes for trichloroethylene degradation in groundwater.
896 Environ. Sci. Technol. 48, 656-663.

897

898 Zeng, T., Zhang, X., Wang, S., Niu, H., Cai, Y., 2015. Spatial confinement of a Co_3O_4
899 catalyst in hollow metal-organic frameworks as a nanoreactor for improved
900 degradation of organic pollutants. Environ. Sci. Technol. 49, 2350-2357.

901

902 Zhao, L., Sun, Z., Ma, J., Liu, H., 2010. Influencing mechanism of bicarbonate on the
903 catalytic ozonation of nitrobenzene in aqueous solution by ceramic honeycomb
904 supported manganese. J. Mol. Catal. A: Chem. 322 (1-2), 26-32.

905

906 Zhang, S. H., Ye, C. S., Lin, H. R., Lv, L., Yu, X., 2015. UV disinfection induces a
907 VBNC state in *Escherichia coli* and *Pseudomonas aeruginosa*. Environ. Sci. Technol.
908 49 (3), 1721-1728.

909

910 Zhang, T., Chen, Y., Wang, Y., Roux, J. L., Yang, Y., Croué, J.-P., 2014. Efficient
911 peroxydisulfate activation process not relying on sulfate radical generation for water
912 pollutant degradation. Environ. Sci. Technol. 48, 5868-5875.

913

914 Zhang, T., Zhu, H., Crou J.-P., 2013. Production of sulfate radical from
915 peroxymonosulfate induced by a magnetically separable CuFe_2O_4 spinel in water:
916 efficiency, stability, and mechanism. Environ. Sci. Technol. 47, 2784-2791.

917

- 918 Zhang, Y., Tran, H. P., Du, X., Hussain, I., Huang, S., Zhou, S., Wen, W., 2017.
919 Efficient pyrite activating persulfate process for degradation of *p*-chloroaniline in
920 aqueous systems: a mechanistic study. Chem. Eng. J. 308, 1112-1119.
921
- 922 Zhong, H., Brusseau, M. L., Wang, Y., Yan, N., Quig, L., Johnson, G. R., 2015.
923 *In-situ* activation of persulfate by iron filings and degradation of 1,4-dioxane. Water
924 Res. 83, 104-111.

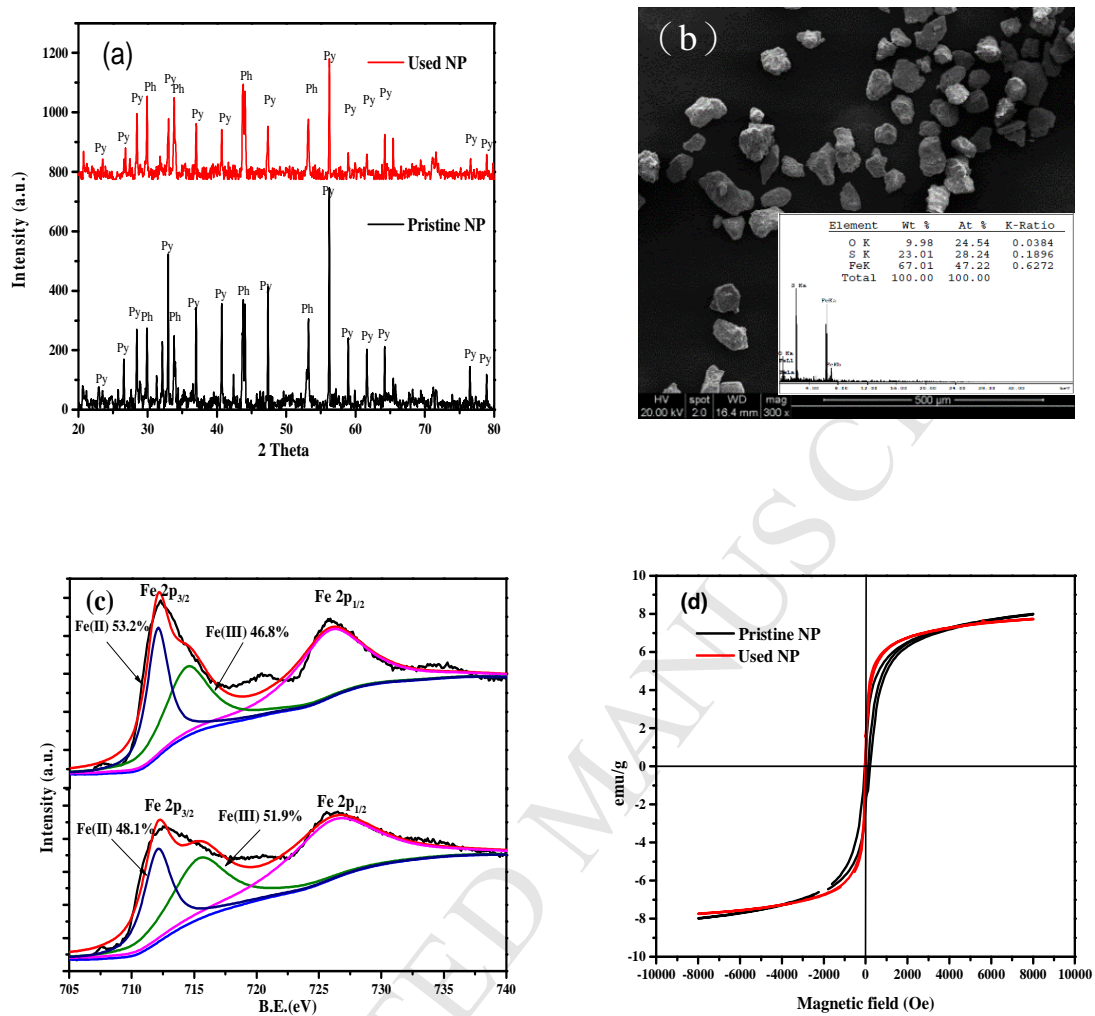
Figures

Fig. 1 (a) XRD, (b) SEM-EDX, (c) XPS spectra and (d) magnetic loops of pristine and recycled NP.

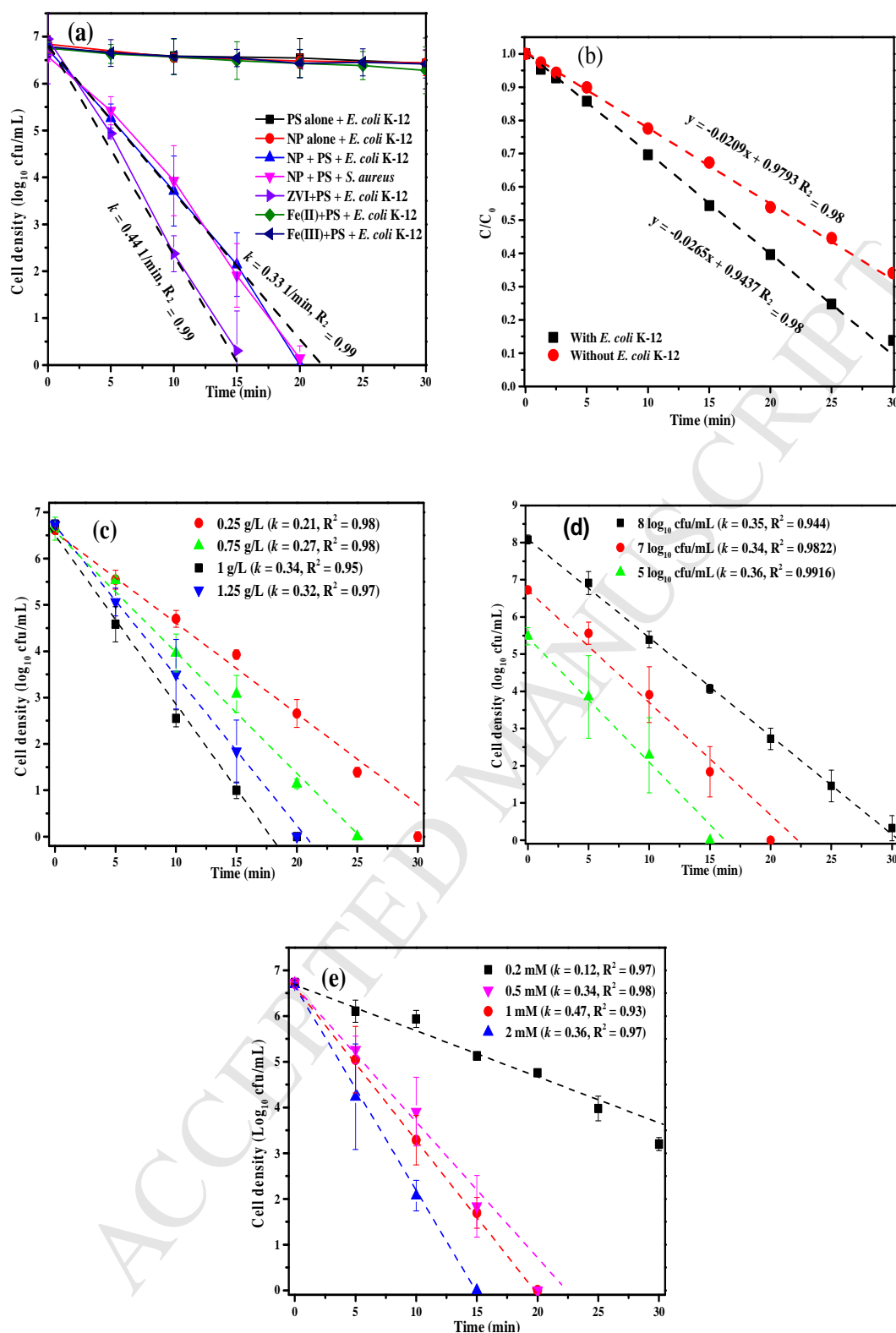


Fig. 2 (a) Sulfate radical-mediated bacterial inactivation in NP/PS system; (b) PS decomposition by NP with and without *E. coli* K-12; Influences of c) NP dose; d) cell density; e) PS concentration on bacterial inactivation by NP/PS system. Experimental conditions: [*E. coli* K-12] = 5-7 \log_{10} cfu/mL, [*S. aureus*] = 7 \log_{10} cfu/mL, [NP] = 0.5-1.25 g/L, [PS] = 0.5-2 mM.

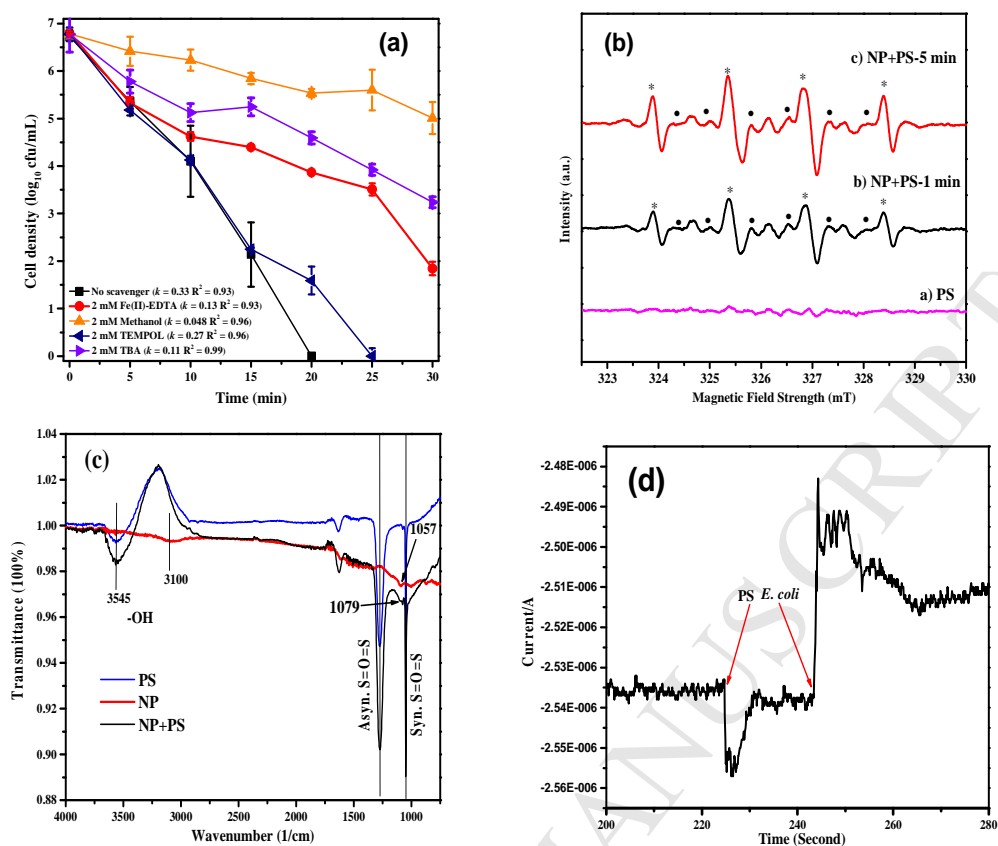


Fig. 3 (a) Scavenger quenching on bacterial inactivation by NP/PS system; (b) ESR spectra of DMPO spin-trapping adducts (asterisk represent DMPO- \cdot OH, and circle represent DMPO- \cdot SO $_4^{2-}$); (c) ATR-FTIR spectra of the PS solution alone, the NP in water, and the NP in PS solution; (d) Chronoamperometric measurements of NP electrode after adding PS and *E. coli* K-12 in turn. Experimental conditions: [*E. coli* K-12] = 7 \log_{10} cfu/mL, [NP] = 1 g/L, [PS] = 0.5 mM.

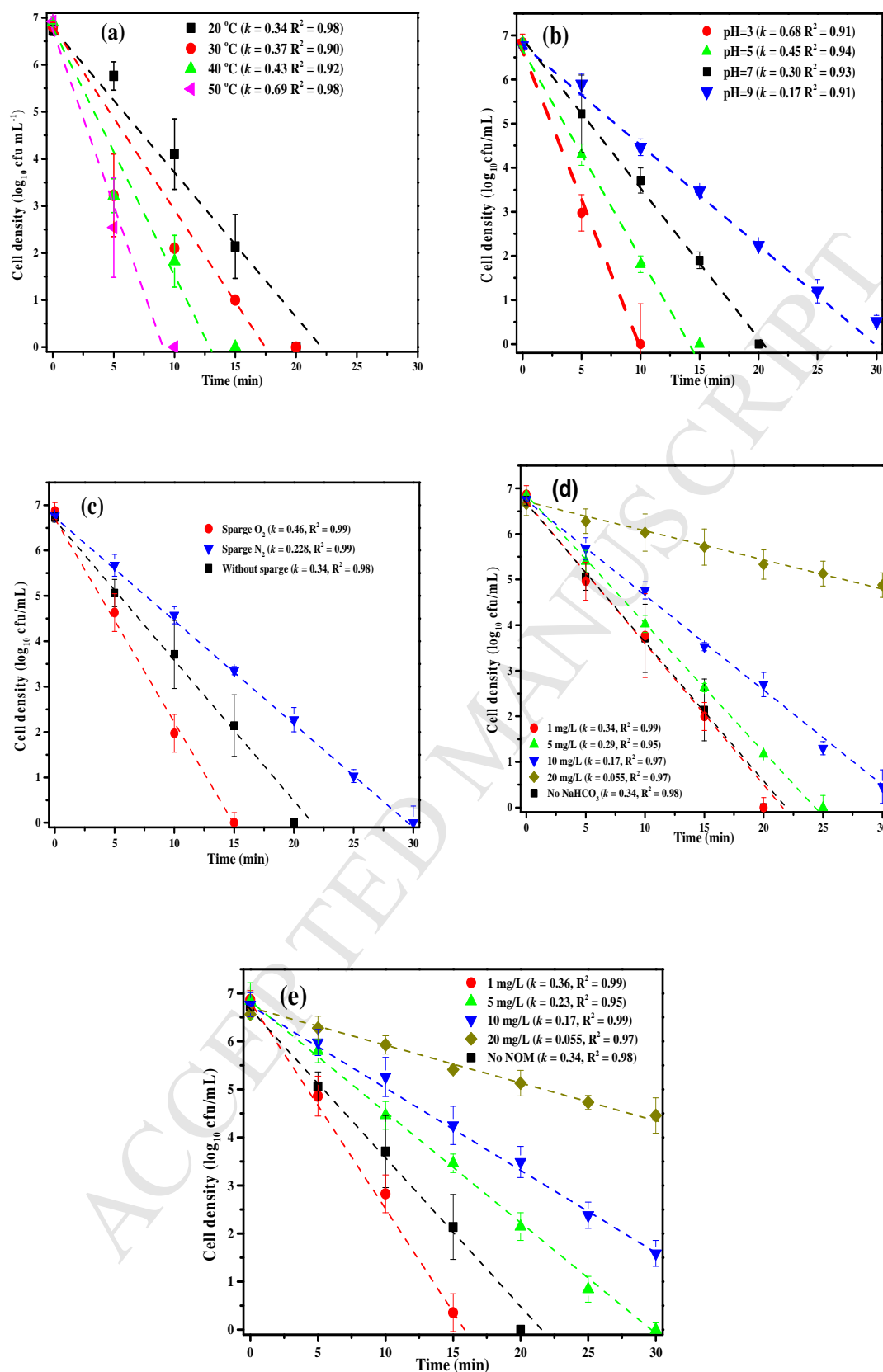


Fig. 4 Influence of a) temperature; b) initial pH; c) dissolved O_2 ; d) $NaHCO_3$; e) natural organic matter on bacterial inactivation by NP/PS system. Experimental conditions: [*E. coli* K-12] = $7 \log_{10}$ cfu/mL, [NP] = 1 g/L, [PS] = 0.5 mM.

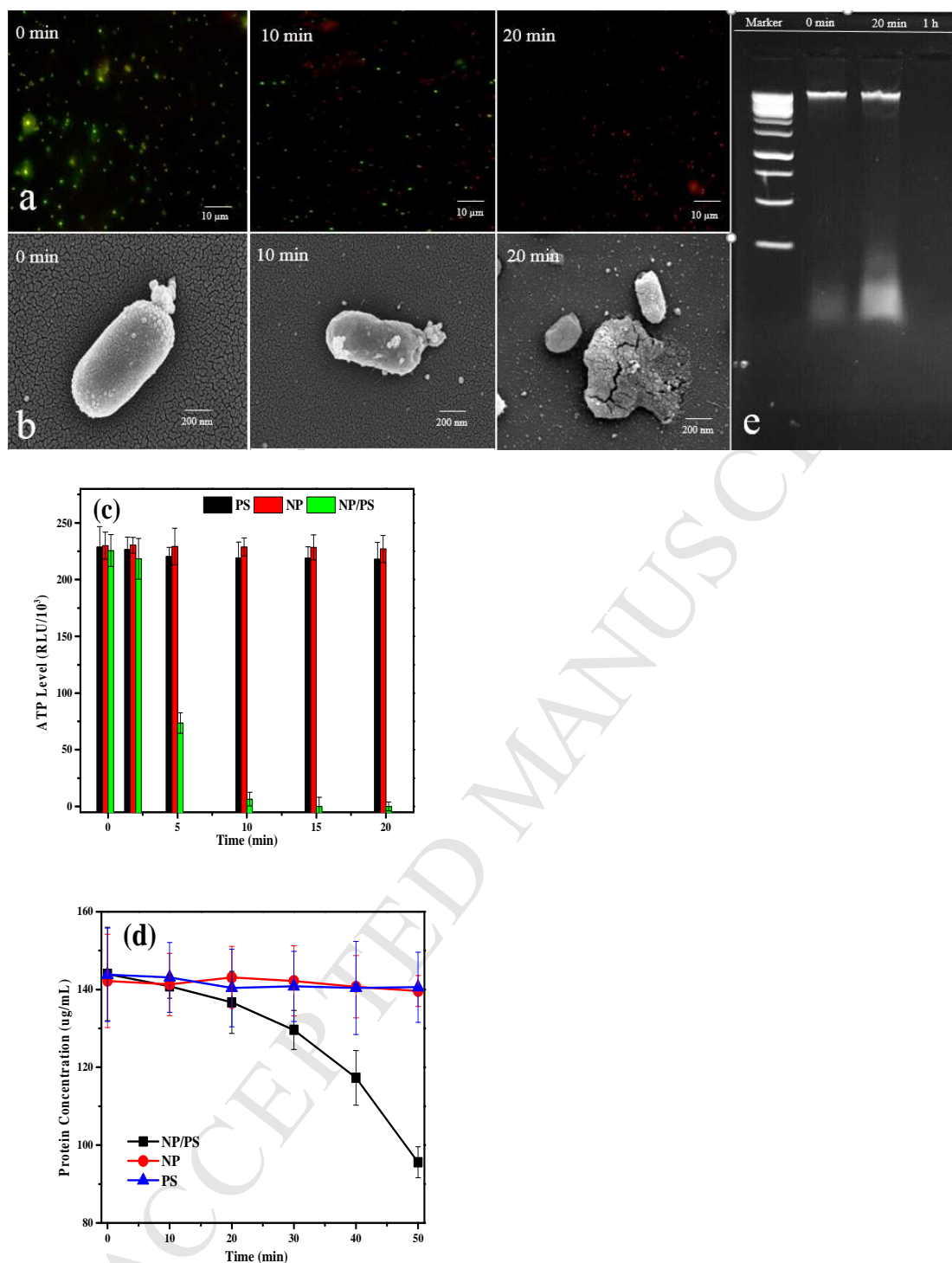


Fig. 5 (a) Fluorescence microscopic images of *E. coli* K-12; (b) SEM images of *E. coli* K-12; (c) ATP content in cells (note: RLU denotes the relative luminescence unit); (d) Detection of protein concentration in 100 μ L concentrated cell lysate from 10 mL bacterial suspension (e) leakage and destruction of bacterial genomic DNA extracted from harvested cells during treatment by NP/PS system. Experimental conditions: [*E. coli* K-12] = 7 log₁₀ cfu/mL, [NP] = 1 g/L, [PS] = 0.5 mM.

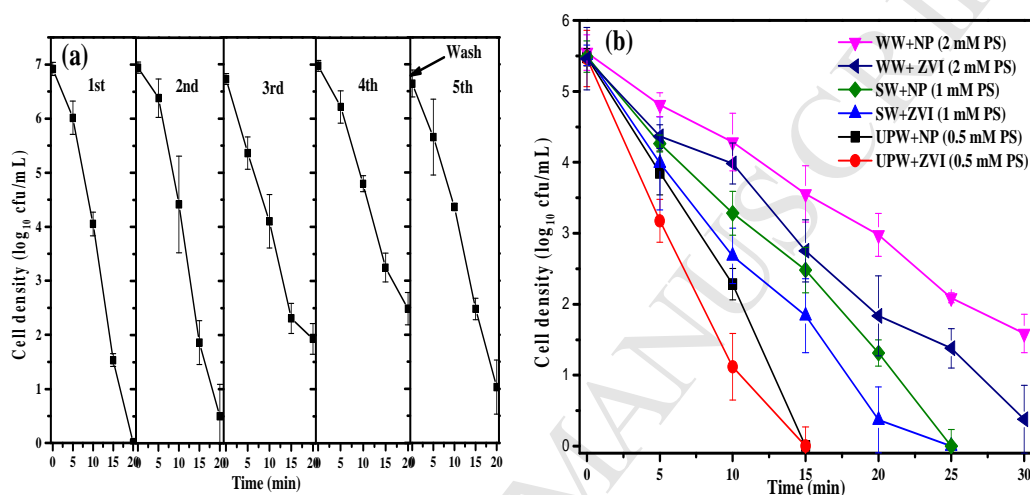


Fig. 6 a) repetitive use of recycled NP for *E. coli* K-12 inactivation; b) inactivation performance in different water matrix with NP/PS and ZVI/PS system. Experimental conditions: [*E. coli* K-12] = 7 log₁₀ cfu/mL, [NP] = 1 g/L, [PS] = 0.5 mM.

Highlights

- Natural magnetic pyrrhotite showed notable catalytic activity to PS.
- Effects of pH, NOM, bicarbonate, oxygen on reactivity of NP/PS were studied.
- The bactericidal role of generated ROS ranked as $\bullet\text{SO}_4^- > \bullet\text{OH} > \text{H}_2\text{O}_2$.
- Charge transfer complex ($\equiv\text{Fe(II)}\cdots\text{O}_3\text{SO-OSO}_3^-$) was formed in NP/PS system.
- Cell-envelope lesions aggravated biomolecular damage to cause bacterial death.